Title

Ovine Models of Congenital Heart Disease and the Consequences of Hemodynamic Alterations for Pulmonary Artery Remodeling

Journal

American Journal of Respiratory Cell and Molecular Biology, 60(5)

ISSN

1044-1549

Authors

Kameny, Rebecca Johnson

Datar, Sanjeev A

Boehme, Jason B

et al.

Publication Date

2019-05-01

DOI

10.1165/rcmb.2018-0305ma

Peer reviewed

Ovine Models of Congenital Heart Disease and the Consequences of Hemodynamic Alterations for Pulmonary Artery Remodeling

Rebecca Johnson Kameny[1], Sanjeev A. Datar[1], Jason B. Boehme[1], Catherine Morris[1], Terry Zhu[1], Brian D. Goudy[1], Eric G. Johnson[2], Csaba Galambos[3], Gary W. Raff[4], Xutong Sun[5], Ting Wang[5], Samuel R. Chiacchia[1], Qing Lu[5], Stephen M. Black[5], Emin Maltepe[1], and Jeffrey R. Fineman[1,6]

[1]Department of Pediatrics and [6]Cardiovascular Research Institute, University of California, San Francisco, San Francisco, California; [2]Department of Veterinary Surgical and Radiological Sciences, School of Veterinary Medicine, and [4]Department of Surgery, University of California, Davis, Davis, California; [3]Departments of Pathology and Laboratory Medicine, University of Colorado School of Medicine, Children's Hospital Colorado, Aurora, Colorado; and [5]Department of Medicine, University of Arizona College of Medicine, Tucson, Arizona

Abstract

The natural history of pulmonary vascular disease associated with congenital heart disease (CHD) depends on associated hemodynamics. Patients exposed to increased pulmonary blood flow (PBF) and pulmonary arterial pressure (PAP) develop pulmonary vascular disease more commonly than patients exposed to increased PBF alone. To investigate the effects of these differing mechanical forces on physiologic and molecular responses, we developed two models of CHD using fetal surgical techniques: *1*) left pulmonary artery (LPA) ligation primarily resulting in increased PBF and *2*) aortopulmonary shunt placement resulting in increased PBF and PAP. Hemodynamic, histologic, and molecular studies were performed on control, LPA, and shunt lambs as well as pulmonary artery endothelial cells (PAECs) derived from each. Physiologically, LPA, and to a greater extent shunt, lambs demonstrated an exaggerated increase in PAP in response to vasoconstricting stimuli compared with controls. These physiologic findings correlated with a pathologic increase in medial thickening in pulmonary arteries in shunt lambs but not in control or LPA lambs. Furthermore, in the setting of acutely increased afterload, the right ventricle of control and LPA but not shunt lambs demonstrates ventricular–vascular uncoupling and adverse ventricular–ventricular interactions. RNA sequencing revealed excellent separation between groups via both principal components analysis and unsupervised hierarchical clustering. In addition, we found hyperproliferation of PAECs from LPA lambs, and to a greater extent shunt lambs, with associated increased angiogenesis and decreased apoptosis in PAECs derived from shunt lambs. A further understanding of mechanical force–specific drivers of pulmonary artery pathology will enable development of precision therapeutics for pulmonary hypertension associated with CHD.

Keywords: pulmonary vascular disease; congenital heart disease; pulmonary hypertension; endothelial dysfunction; mechanical forces

Pulmonary vascular disease (PVD) associated with congenital heart disease (CHD) remains an important source of morbidity and mortality worldwide (1–3). Although often considered as a single entity, pulmonary vascular pathology associated with CHD comprises a complex and varied pathophysiology, dependent on the associated hemodynamic aberrations (4, 5). The natural history of PVD associated with CHD reveals the differential—or perhaps incremental—effects of increased pulmonary blood flow (PBF) and increased pulmonary arterial pressure (PAP). In patients with increased PBF alone, as

(Received in original form September 14, 2018; accepted in final form January 4, 2019)

Supported in part by grants from the National Institutes of Health (HL61284, R01 HL137282 [J.R.F. and S.M.B.], R01 HD072455-05 [E.M.], and RO1 HL133034 [S.A.D.]), the American Heart Association (14FTF19670001 [R.J.K.]), the Pulmonary Hypertension Association (Robyn J. Barst Pediatric Pulmonary Hypertension Research and Mentoring Grant [R.J.K.]), and Entelligence MD (Entelligence Young Investigator grant [R.J.K.]).

Author Contributions: Conception and design of study: R.J.K., S.A.D., E.M., and J.R.F.; data acquisition, analysis, and interpretation: R.J.K., S.A.D., J.B.B., C.M., T.Z., B.D.G., E.G.J., C.G., G.W.R., X.S., T.W., S.R.C., Q.L., S.M.B., E.M., and J.R.F.; and drafting of the manuscript for important intellectual content: R.J.K., S.A.D., S.M.B., E.M., and J.R.F.

Correspondence and requests for reprints should be addressed to Rebecca Johnson Kameny, M.D., Department of Pediatrics, University of California, San Francisco, 513 Parnassus Avenue, HSE 1401, San Francisco, CA 94941. E-mail: rebecca.johnson@ucsf.edu.

This article has a data supplement, which is accessible from this issue's table of contents at www.atsjournals.org.

Am J Respir Cell Mol Biol Vol 60, Iss 5, pp 503–514, May 2019

Originally Published in Press as DOI: 10.1165/rcmb.2018-0305MA on January 8, 2019
Internet address: www.atsjournals.org

associated with pre–tricuspid valve shunts such as atrial septal defects, the development of PVD is uncommon and presents late, among 5–15% of patients by the fourth decade of life (6, 7). Conversely, in patients exposed to increased PBF and PAP, as associated with post-tricuspid shunts such as ventricular septal defects, PVD is common, progressive, and develops early in life (3, 8, 9). The different hemodynamic forces associated with different CHD lesions are presumed to account for observed differences in natural history of PVD; however, the underlying pathobiological mechanisms are unknown.

Despite rapid advancement in the number of therapies available to treat PVD, mechanistic therapeutic targets remain limited, and outcomes remain suboptimal. In fact, current treatment regimens for pulmonary hypertension are generally based on illness severity rather than on underlying mechanisms (10–12). Although most pulmonary vascular therapies target the distal pulmonary vascular bed, the importance of increased stiffness in the proximal or conducting pulmonary arteries is increasingly recognized as an important mediator of PVD. For example, increased stiffness within the larger conducting pulmonary vessels is associated with a greater increase in right ventricular (RV) afterload than total pulmonary vascular resistance (13), and pulmonary artery (PA) stiffness is correlated with survival among children and adults with pulmonary hypertension (14, 15). In addition, decreased distensibility in conducting PAs propagates increased pulse wave velocity to the distal pulmonary vascular bed, and mechanotransduction within pulmonary artery endothelial cells (PAECs) in the proximal pulmonary vessels is sensitive to alterations in stiffness of the vascular matrix (16). Thus, investigation of the effect of hemodynamic forces on conducting PAEC biology has important pathobiological and therapeutic implications.

Previously, we created a model of increased PBF and pulmonary pressure by placing a large GORE-TEX graft (W. L. Gore & Associates, Inc.) between the ascending aorta and PA in late-gestation fetal lambs (17). This well-established model mimics lesions such as a large ventricular septal defects, and the biochemical and gene expression alterations described also mimic infants with CHD (18). The purpose of this study was to establish a novel ovine model of CHD with increased PBF alone through fetal left pulmonary artery (LPA) ligation and to compare the effects on the pulmonary vasculature of this increased PBF with our shunt model with increased postnatal PA pressure and flow. To our knowledge, this study is the first to characterize the anatomic, physiologic, histologic, and transcriptomic changes associated with increased PA pressure and flow compared with increased PBF alone. Furthermore, given the essential role of endothelial cell function and proximal PA stiffness in both normal pulmonary vascular physiology and pathology, we isolated primary PAECs from the proximal PAs and defined their transcriptomic expression profile as well as proliferative capabilities. Together, these data are the first to provide insight into alterations in pulmonary vascular biomechanical forces associated with different types of CHD and associated changes in endothelial cell function. A portion of the work described in this article was presented in abstract form at the Pediatric Academic Societies Meeting in 2018 (19).

Methods

Animal Care

Animal care is described in detail in the data supplement. All protocols and procedures were approved by the Committee on Animal Research at the University of California, San Francisco.

Surgical Preparation and Reactivity Testing

Detailed surgical preparation for both the fetal LPA ligation and shunt models is provided in the data supplement. Briefly, late-gestation (~135 d) fetal lambs underwent lateral thoracotomy followed by placement of either an 8-mm GORE-TEX graft between the ascending aorta and main PA or ligation and division of the LPA. After fetal surgery, pregnant ewes recovered, and lambs underwent spontaneous vaginal delivery 1–2 weeks after surgery. Unoperated twin lambs served as control animals. Lambs then underwent hemodynamic study at 4–6 weeks of age, including vascular reactivity testing. *See* the data supplement for details.

Imaging

The computed tomographic imaging procedure is described in detail in the data supplement.

PA Isolated Vessel Baths

PA ring segments were mounted in myograph chambers and treated with increasing concentrations of norepinephrine. *See* the data supplement for details.

Medial Thickness Determination

Briefly, right lower lobe segments were analyzed from five animals in each experimental group. PA vessels of 100 μm or less were analyzed; 5–10 vessels were analyzed from each animal; and three to eight measurements taken per vessel. *See* the data supplement for further details.

Pressure–Volume Loop Analysis

Pressure–volume loop analysis of myocardial performance has previously been described in detail (20) and is further delineated in the data supplement.

Cell Culture, Apoptosis, and Proliferation

PAECs were isolated and cultured as previously described (21). Briefly, primary PAECs were isolated via the explant technique from the main PA. A segment of the main PA was placed in a sterile dish containing Dulbecco's modified Eagle medium with appropriate supplementation. The segment was stripped of adventitia with sterile forceps and opened longitudinally, and the endothelial layer was removed by gentle rubbing with a cell scraper. Cells were grown in culture in appropriate media. After several days, moderate-sized aggregates of endothelial cells were transferred using a micropipette, grown to confluence, and then maintained in culture. Further details and methods used for apoptosis and proliferation quantification are provided in the data supplement.

RNA-Sequencing Analysis

RNA-sequencing and global analyses were performed by Exiqon. In addition, we used the Gene Ontology (GO) database to investigate which biological processes were significantly enriched with differentially expressed transcripts (DETs). Further details are provided in the data supplement.

Statistical Analysis

Changes within each animal before and after an intervention were compared by the paired *t* test, and changes between groups were compared by the unpaired *t* test. Nonparametric testing was used when appropriate. Variables were compared between multiple groups or within each group over time by ANOVA for repeated measures. Student-Newman-Keuls *post hoc* testing was performed. $P < 0.05$ was considered significant. Statistical analysis was done using Prism 7.0d software (GraphPad Software, Inc.).

Results

After establishing our surgical models, we defined the morphology of the three models in juvenile lambs (3 wk of age) using computed tomography angiography (CTA) (Figure 1). CTA of control animals demonstrated the expected size ratio between aorta and PA with a normal vascular arborization pattern. In contrast, the CTA of the fetal LPA ligation lamb shows an expected complete absence of the LPA and left distal vasculature with mild dilation of the remaining right main PA and branches. Finally, CTA of the shunt lamb demonstrates marked dilation of the main PA segment with dilation and extended recruitment of distal vessels, compared with control.

When lambs from each model system were 4–6 weeks of age, they underwent a terminal hemodynamic study and *in vivo* pulmonary vascular reactivity testing (Table 1). There were no differences in age and weight between the model lambs at the time of study (data not shown). As expected, both LPA and shunt lambs had significantly higher right pulmonary artery blood flow than control animals, although right PA blood flow was twofold control in LPA lambs, and threefold control in shunts. Although LPA lambs had modest increases in mean PAP compared with control animals (19 ± 3.6 vs. 14 ± 1.8 mm Hg, respectively), PAP was significantly higher in shunt lambs (26 ± 6.3 mm Hg; $P < 0.01$) than in both control and LPA lambs. Furthermore, shunt lambs had increased pulmonary pulse pressure and greater difference between diastolic and systolic pressure compared with both control and LPA lambs, whereas pulmonary pulse pressure was similar in control and LPA lambs. This physiologic difference has important pathologic consequences, given the increase in cyclic stretch associated with pulse pressure (22, 23).

Having established baseline hemodynamics, we next administered pulmonary vasoconstricting stimuli and assessed differing responses in the intact animals. In response to hypoxia (Fi_{O_2}, 10%), shunt lambs had significantly increased mean PAP compared with both control and LPA lambs. Next, we administered the thromboxane A_2 mimic U46619 via continuous infusion (1 μg/kg/min) to induce pulmonary vasoconstriction. After 10 minutes, LPA lambs had a greater rise in mean PAP than did control lambs, but the increase in PAP was even higher in shunt lambs (Figure 2A). This was not associated with a decrease in RV contractility as quantified by end-elastance (Ees) (Figure 3A). Then, we isolated fifth-generation PAs and assessed vasomotor reactivity using a wire myograph system (DMT). In response to increasing concentrations of norepinephrine (1×10^{-9} to 3×10^{-6} M), all groups had an increase in developed tension, as expected, but this increase was significantly more pronounced in PA rings obtained from shunt animals than in PA rings from control or LPA animals (Figure 2B). Together, these data suggest that shunt animals have exaggerated pulmonary vascular reactivity compared with controls and that LPA ligation lambs have an intermediate phenotype with some increased sensitivity to U46619 that was not evident with other vasoconstricting stimuli.

Having assessed *in vivo* vascular reactivity, we next sought to measure cardiac performance using pressure–volume loop analyses. We previously demonstrated that the right ventricle in shunt lambs has a unique ability to increase contractility in response to acute increases in afterload due to PA banding (20). In this study, U46619 was administered to increase RV afterload and was maintained for several minutes; a family of pressure–volume loops was then generated by manipulating preload with transient inferior vena cava occlusion. Contractility was quantified using the slope of the end-systolic pressure–volume relationship (Ees). In response to increased afterload, only shunt animals had a significant increase in RV Ees (3.4 ± 0.4-fold baseline) compared with control and LPA ligation animals (1.6 ± 0.5- and 0.8 ± 0.5-fold baseline, respectively) (Figure 3A). Furthermore, we assessed ventricular–vascular coupling, which is quantified via the relationship between Ees and arterial elastance (Ea). As shown in Figure 3B, both control and LPA animals showed ventricular–vascular uncoupling after acutely increased RV afterload (U46619); control and LPA RV Ees/Ea were both significantly decreased compared with baseline (0.5 ± 0.2- and 0.6 ± 0.01-fold baseline, respectively), whereas shunt animals maintained ventricular–vascular coupling with preserved RV Ees/Ea ratio (0.9 ± 0.7-fold baseline). These findings are consistent with

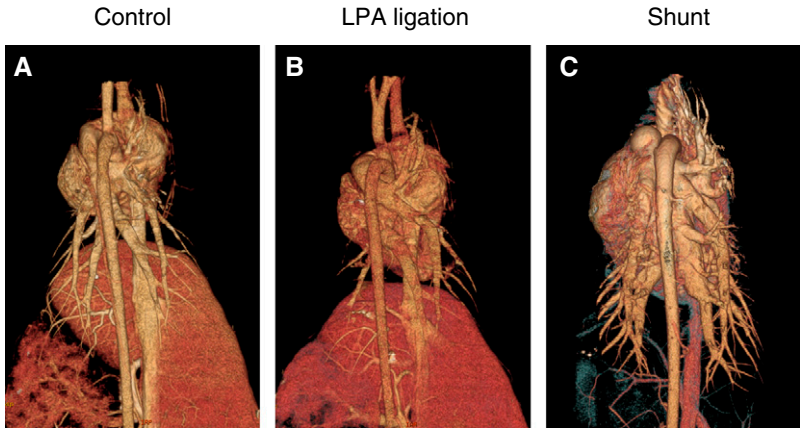

Figure 1. Three-dimensional reconstruction of computed tomography angiography of representative (*A*) control, (*B*) left pulmonary artery (LPA), and (*C*) shunt lambs. Images are shown from the posteroanterior perspective. LPA lamb computed tomography angiography demonstrates expected hypoplasia of the LPA and veins. Shunt lamb computed tomography demonstrates dilation of main pulmonary artery root with marked dilation of the distal left and right pulmonary arteries.

Table 1. Baseline Hemodynamics in Control, Left Pulmonary Artery Ligation, and Shunt Lambs

	SBP (*mm Hg*)	DBP (*mm Hg*)	MAP (*mm Hg*)	HR (*beats/min*)	PA SBP (*mm Hg*)	PA DBP (*mm Hg*)	mPAP (*mm Hg*)	ΔPAP (*mm Hg*)	RPAQ (*L/min*)
Control ($n = 9$)	97 ± 12	57 ± 8.6	70 ± 9.4	118 ± 21	20 ± 3.4	8.5 ± 1.6	14 ± 1.8	11.8 ± 0.2	0.7 ± 0.1
LPA ($n = 8$)	106 ± 17	58 ± 14	74 ± 15	121 ± 16	27 ± 5.2*	12 ± 3.3*	19 ± 3.6*	14.8 ± 3.2	1.4 ± 0.3*
Shunt ($n = 4$)	118 ± 5.7*	36 ± 8.5*	61 ± 8.7	126 ± 17	35 ± 9.2*†	18 ± 5.1*†	26 ± 6.3*†	18 ± 0.4*†	2.0 ± 0.2*†

Definition of abbreviations: ΔPAP = pulse pulmonary pressure; DBP = diastolic blood pressure; HR = heart rate; LPA = left pulmonary artery; MAP = mean arterial pressure; mPAP = mean pulmonary arterial pressure; PA = pulmonary artery; RPAQ = right lung pulmonary artery blood flow; SBP = systolic blood pressure.
In order to compare pulmonary blood flow between the three groups, RPAQ was estimated assuming 55% of total pulmonary blood flow for control and shunt lambs.
*$P < 0.05$ versus control animal.
†$P < 0.05$ shunt versus LPA ligation lambs.

our previous study but represent important new findings because the type of afterload challenge is different, with U46619 resulting in more diffuse increases in vascular impedance in contrast to the discrete afterload resulting from PA banding.

Next, given the adverse effects that RV dysfunction can have on left ventricular (LV) filling, we examined indices of LV diastolic function, particularly LV stiffness, which is derived from the nonlinear slope of the LV end-diastolic pressure–volume relationship. In the presence of the thromboxane A_2 mimic, U46619, PAP—and thus RV afterload—increases significantly in all groups, as shown in Figure 3A. LV afterload increases more modestly (~20%) above baseline. During U46619 administration, LV stiffness increases to 151 ± 47% of baseline in control animals and 154 ± 7% of baseline in LPA lambs, whereas LV stiffness decreases to 75 ± 5% of baseline in shunt animals (Figure 3C). Under baseline conditions, LV volume rapidly rises during early diastole with a smooth upstroke in all three models. In contrast, with the addition of RV afterload due to U46619, LV filling in control and LPA lambs, but not in shunt lambs, has a biphasic filling pattern with early rapid filling that plateaus followed by a second phase to complete LV end-diastolic volume in late diastole due to atrial kick (Figure 3D). This is indicative of impaired LV diastolic function in the face of RV afterload in control and LPA lambs but not in shunt lambs. Steady-state data under both baseline conditions and with increased RV afterload are available in Table E1 in the data supplement, together with representative pressure–volume loops in Figure E1.

Given our observations of increased pulmonary vasoreactivity in shunt lambs, we next examined pulmonary arteries histologically for medial hypertrophy. ACTA2 staining was performed on 5–10 pulmonary arteries of diameter 100 μm or less from each animal. Medial thickness of pulmonary arteries was significantly increased in shunt lambs (12.9 ± 2.8 μm) compared with both control (7.4 ± 0.4 μm) and LPA lambs (9.2 ± 1.1 μm) (Figure 4). Our findings of increased PA muscularization are consistent with prior studies of shunt lambs (17) and our *in vivo* and *ex vivo* vascular reactivity data.

Having defined the cardiovascular and pulmonary vascular physiologic response to differing chronic hemodynamic forces in

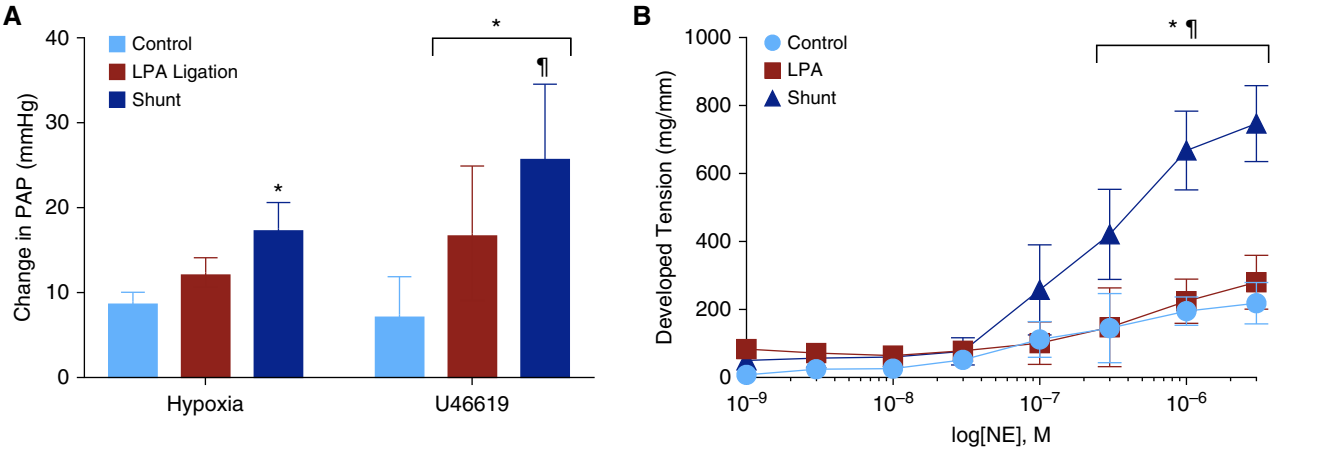

Figure 2. Shunt animals have exaggerated pulmonary vascular reactivity. (*A*) After 10 minutes of hypoxia (fraction of inspired oxygen, 10%), mean pulmonary artery pressure (PAP) increases by 9.0 ± 1.1 mm Hg in control, 12.4 ± 1.7 mm Hg in LPA, and 17.6 ± 3.0 mm Hg in shunt lambs. With administration of thromboxane A_2 mimic, U46619 via continuous infusion 1 μg/kg/min, mean PAP increases by 6.7 ± 4.8 mm Hg in control, 17 ± 7.9 mm Hg in LPA, and 25 ± 8.6 mm Hg in shunt lambs. $n = 7$ control, $n = 7$ LPA, and $n = 5$ shunt. (*B*) Fifth-generation pulmonary arteries were isolated, mounted, and prestretched. Increasing concentrations of norepinephrine (NE) were added (1×10^{-9} to 3×10^{-6} M). Pulmonary artery rings isolated from shunt lambs generated significantly higher force at NE concentrations of 3×10^{-7} up to 3×10^{-6} M than did pulmonary artery rings isolated from control or LPA lambs. $n = 5$ in each group. Error bars represent ±SD. *$P < 0.05$ compared with control and ¶$P < 0.05$ compared with LPA.

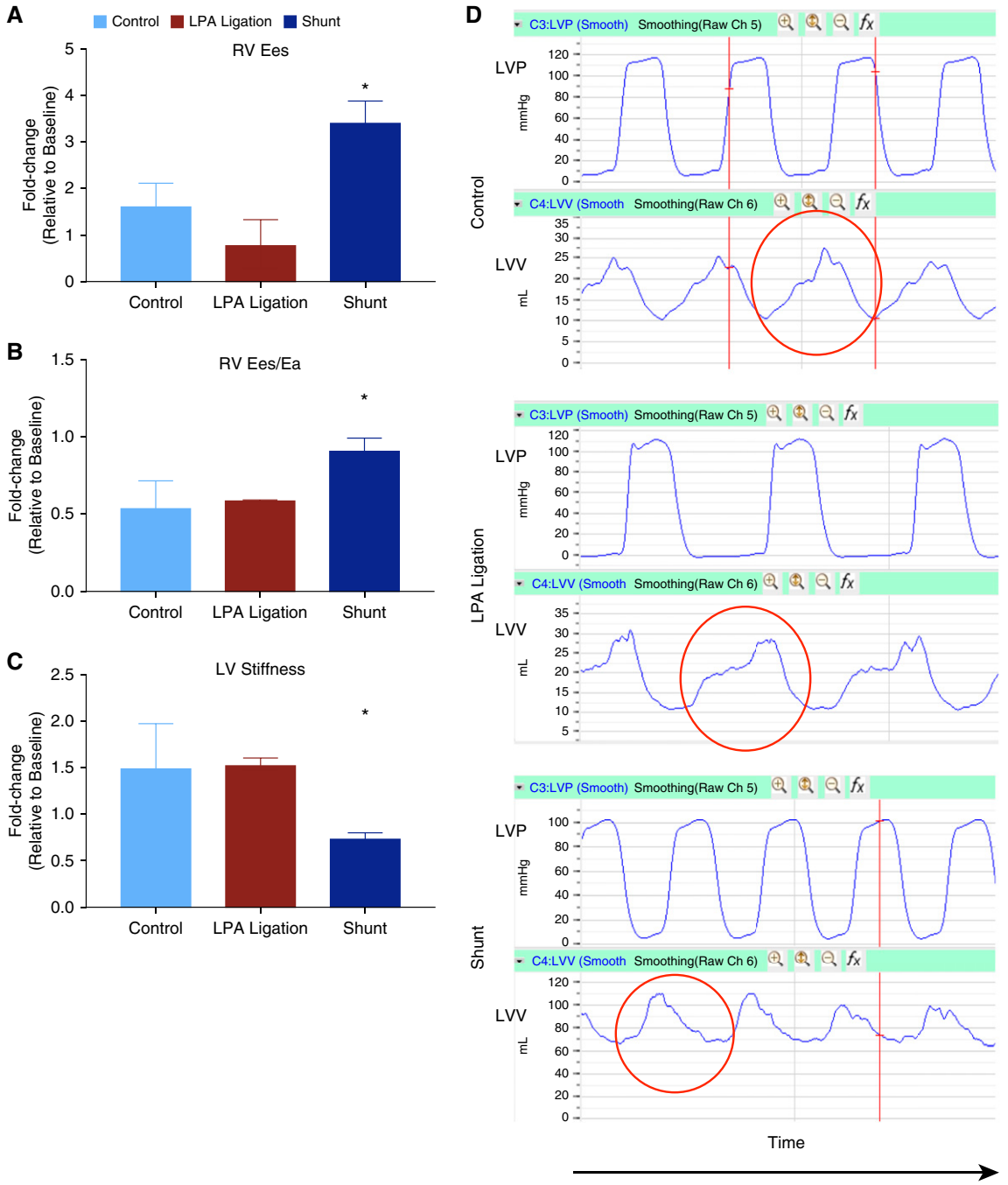

Figure 3. Shunt animals have superior right ventricular (RV) and left ventricular (LV) myocardial performance after U46619 administration. RV contractility, ventricular–vascular coupling, and LV diastolic function were quantified in all three groups at baseline and after the administration of the thromboxane A_2 mimic, U46619, which significantly increases RV afterload and modestly increases LV afterload. (*A*) RV contractility was quantified by the slope of the end-systolic pressure–volume relationship, end elastance (Ees). Compared with baseline, shunt animals significantly increased RV Ees after U46619 administration, whereas control and LPA animals did not have significant change in RV Ees from baseline. (*B*) Ventricular–vascular coupling was quantified by the ratio of Ees to arterial elastance (Ea). Control and LPA animals had ventricular–vascular uncoupling after U46619 administration, whereas shunt animals maintained baseline RV Ees/Ea ratio. (*C*) Diastolic function was quantified using LV stiffness, the nonlinear slope of the LV end-diastolic pressure–volume relationship. After U46619 administration, LV stiffness increased in control and LPA animals, whereas LV stiffness decreased in shunt animals. (*D*) After U46619 administration, in control and LPA animals, but not in shunt animals, LV filling over time changed from a smooth upstroke to a biphasic pattern with an early plateau followed by a second filling period to end-diastolic volume due to atrial kick. Shunt animals did not have a change in LV filling. Error bars represent 1 ± SD. *$P < 0.05$ compared with control. LVP = left ventricular pressure; LVV = left ventricular volume.

our model, we next sought to examine the gene expression profile of PAECs, which are primarily affected by both shear (increased PBF) and cyclic stretch (increased pulmonary pressure). We first performed RNA sequencing on PAECs derived from control, LPA, and shunt lambs. Principal clustering analysis (Figure 5A) demonstrated excellent differentiation between PAECs derived from each model, as did dendrogram and unsupervised hierarchical clustering heat map analysis (Figure 5B). We next visualized comparisons between each individual group using volcano plots representing the relationship between fold change and significance. Volcano plots are shown in Figure 5 for control versus LPA animals (Figure 5C), control versus shunt animals (Figure 5D), and LPA versus shunt animals (Figure 5E). These data provide visualization for transcriptome-level differences between models. Although important differences exist, the LPA ligation model (increased PA flow only) is the most similar to control, whereas shunt lambs (increased PA pressure and flow) have more differences in RNA expression, in terms of both significance and fold change. Top DETs among models are detailed in Tables E2–E4. Taken together, these data confirm that our observations of different physiologic responses are also evident at the transcriptional level in PAECs derived from these models.

Given the clear physiologic changes observed in shunt lambs, we hypothesized that the scale of transcriptional changes would be largest in shunt PAECs. Indeed, this was the case: 609 transcripts were found to be upregulated in shunt PAECs relative to control cells and 947 downregulated transcripts. There were relatively fewer DETs observed in the comparison of LPA and control PAECs in which 47 transcripts were found to be upregulated and 147 were found to be downregulated. Figures 6A and 6B illustrate the number of DETs shared between each of the three comparisons, revealing that there are a number of up- and downregulated DETs shared between LPA and shunt PAECs, —suggesting that similar transcriptional pathways might be impacted in response to increased PBF in both LPA ligation and shunt lambs.

We next used the GO database to characterize differences in up- and downregulated genes in our models. Among the 180 upregulated DETs in shunt lambs that were distinct from both control and LPA lambs, 131 could be mapped to human homologs. These genes significantly enriched 153 GO terms, a number of which are especially relevant to pulmonary hypertension pathophysiology, including angiogenesis (GO:0001525) and vascular development (GO:0001944), as illustrated in Figure 6C. The majority of these terms (75%) were associated with cell cycle and proliferation—, providing transcriptional evidence of the hyperproliferative phenotype unique to shunt PAECs. Additional pathways of interest include the negative regulation of apoptosis (GO:0043066) and the positive regulation of protein metabolism (GO:0019538) (Figures 6D and 6E). This phenotype is best captured by the 27 DETs that significantly enrich the term "Mitotic M-Phase" (GO:0000087) illustrated in Figure 6F. Of the 362 downregulated DETs at this intersection, 219 could be mapped to human homologs. These 219 genes enriched 219 pathways—, the majority of which were associated with organ development, metabolism, and biosynthesis. Ultimately, this pathway analysis works to demonstrate the effect of increased pressure and flow on gene expression in PAECs, indicating that aberrant hemodynamic conditions contribute to the differential expression of genes that likely play a role in the development of the PVD.

Given that PAECs derived from these CHD models have important transcriptome differences, we next defined the functional characteristics of PAECs derived from these different lamb models. We first used a tube formation assay in growth factor–restricted Matrigel to characterize angiogenesis. PAECs from LPA ligation animals had a greater rate of angiogenesis than control animals after 72 hours in Matrigel, as quantified by the number of branch points. However, PAECs derived from shunt animals had an even greater rate of angiogenesis than did either control or LPA animals (Figure 7A). Next, we quantified apoptosis using terminal deoxynucleotide transferase–mediated dUTP nick end label staining after tumor necrosis factor-α stimulation to induce apoptosis. Control PAECs had the greatest percentage of apoptotic cells, followed by LPA PAECs, with shunt PAECs exhibiting the greatest resistance to apoptosis (Figure 7B). Then, we used two different methodologies, cell counting and 5′-bromo-2′-deoxyuridine incorporation, to quantify PAEC proliferation from each model. We found that both total cell count (Figure 6C) and 5′-bromo-2′-deoxyuridine incorporation (Figure 6D) demonstrated greater proliferation in PAECs derived from shunt animals than both control and LPA ligation animals. Consistent with other models of PVD (24, 25), these data collectively demonstrate that PAECs derived from shunts are more proliferative, apoptosis-resistant, and prone to angiogenesis than PAECs derived from either control or LPA ligation lambs, although PAECs derived from LPA ligation lambs do have an intermediate phenotype, compared with control and shunt animals, in their resistance to apoptosis and propensity for angiogenesis.

Discussion

The natural history of PVD associated with CHD suggests distinct pathophysiologic consequences of different hemodynamic insults to the pulmonary vasculature. In this study, we established the first fetal cardiac surgical model of increased PBF alone (LPA ligation) and compared that new model with our established CHD model of increased pulmonary pressure and flow (shunt lambs). These studies demonstrated substantial differences between the animals with normal physiology, those with increased PBF (LPA), and those with increased pulmonary pressure and flow (shunt), both in whole-animal physiologic responses to vasoactive stimuli and in the proximal PAEC transcriptome. These large animal models represent a seminal development in the ability of preclinical studies of PVD associated with CHD to characterize responses in the intact animal as well as endothelial cells derived from primary cell culture.

This study links whole-animal physiology, cardiac and pulmonary hemodynamics, microanatomy, and specific PAEC properties. PAECs are constantly under the influence of hemodynamic forces, including shear stress, the tangential friction force acting on the vessel wall due to blood flow (26); hydrostatic pressure, the perpendicular force acting on the vascular wall (27); and cyclic strain, the circumferential stretch of the vessel wall (28). Mechanosensors on these cells detect

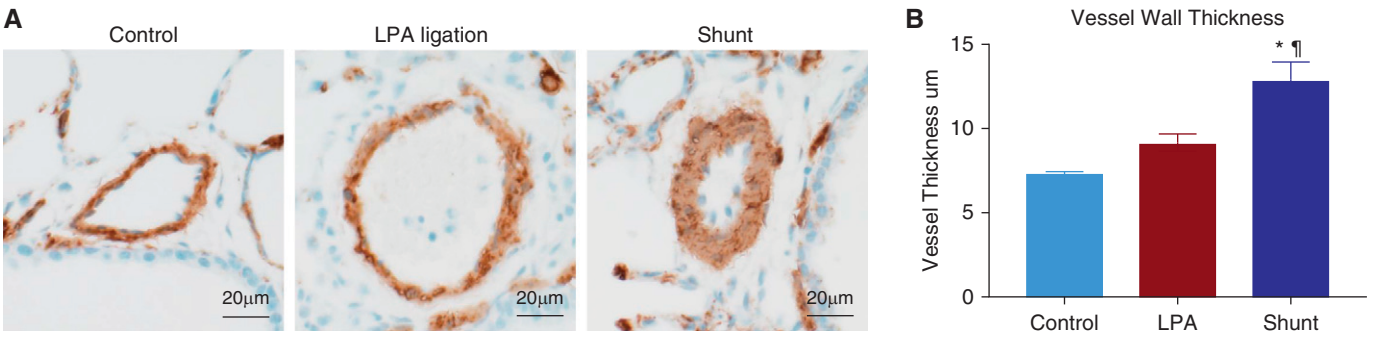

Figure 4. Shunt animals have increased pulmonary vessel medial wall thickness. Shunt animals demonstrate more medial vessel wall thickness than control and LPA animals. (*A*) Smooth muscle actin staining of pulmonary artery walls was performed. Images shown are representative of 5–10 vessels/animal ($n = 5$ in each group). (*B*) Three to eight measurements were taken per vessel. Pulmonary arteries from shunt animals had the greatest medial wall thickness (12.9 ± 2.8 μm) compared with control (7.4 ± 0.4 μm) and LPA (7.7 ± 1.1 μm) animals. Error bars represent 1 ± SD. $^{*}P < 0.05$ compared with control and $^{¶}P < 0.05$ compared with LPA. Scale bars: 20 μm.

these forces and transduce them into biochemical signals that trigger vascular responses and ultimately pathologic hyperreactivity in PVD (29). Among the various force-induced signaling molecules, alterations in nitric oxide (NO), reactive oxygen species (ROS), and endothelin 1 (ET-1) have been implicated in vascular health and disease (30). Normal physiologic conditions result in induction of NO production with decreased ROS and ET-1, whereas pathologic conditions result in decreased NO with increased ROS and ET-1 (31).

Mechanotransduction in endothelial cells differs with both developmental stage and vascular bed. As a consequence of *in vivo* mechanical forces, PAECs derived primarily from these CHD models maintain their phenotype in culture for several passages, as evinced by differing angiogenesis, proliferation, and sensitivity to apoptotic stimuli (Figure 7). The persistent differences in PAECs from different animal models in cell culture implicates epigenetic changes as a mechanism for phenotypic preservation and furthermore makes future targeted mechanistic investigation of mechanosensing pathways in PAECs feasible.

As expected, given the differing mechanical forces accompanying each model's physiology, the most dramatic differences in endothelial function and vascular responses were evident among whole-animal responses and PAEC characteristics in shunt animals compared with the control or LPA ligation models. However, the LPA ligation model demonstrated a primed or intermediate phenotype in endothelial function, which possibly reflects chronic effects of flow-mediated shear stress. For example, LPA ligation animals demonstrated intermediate increases in pulmonary vasoconstriction response to hypoxia and U46619; similarly, PAECs derived from LPA ligation animals demonstrated an intermediate degree of angiogenesis and proliferation compared with PAECs derived from control and shunt lambs. Furthermore, global visualization of whole-transcriptome data from these animal models demonstrated significant expression differences in PAECs between control, LPA ligation, and shunt lambs (Figure 5). These findings of an intermediate phenotype are consistent with clinical experience, which suggests that the stimulus of increased PBF alone is not sufficient to develop significant, rapidly progressive PVD, but these patients may be more vulnerable to "second hits" such as predisposing genetic conditions, environmental hypoxia due to living at altitude or lung disease, or diseases leading to vascular inflammation.

The role of angiogenesis and vascular cell proliferation in the pathogenesis of PVD is complex with both early adaptive and late maladaptive sequelae. Early angiogenesis or capillary recruitment in the setting of CHD lesions with increased PBF increases the cross-sectional area of the pulmonary vascular bed and thus decreases shear forces at the capillary level and maintains low pulmonary vascular resistance despite increased PBF. Indeed, we previously demonstrated increased numbers of arterioles in juvenile lambs in our shunt CHD model compared with control animals (17). However, increased PAEC proliferation and resistance to apoptosis, as demonstrated in PAECs derived from LPA lambs, and especially shunt lambs, does not necessarily reflect adaptive angiogenesis. For example, highly proliferative endothelial cells and complex intravascular lesions with luminal obstruction as a consequence of monoclonal expansion of antiapoptotic endothelial cells—plexiform lesions—have been isolated from humans with advanced PVD (32, 33). Our histologic examination of lungs from these CHD models revealed only medial hypertrophy (vascular smooth muscle cell proliferation) and no evidence of either endothelial obliteration of the vessel lumen or plexiform lesions. However, it is possible that the proliferative, antiapoptotic phenotype seen in shunt PAECs is a precursor to this advanced pathology.

Increasingly, understanding of PVD has broadened to consider the RV and pulmonary vasculature together as a functional unit, and outcomes in patients with PVD correlate with RV function (34). On the basis of the present study, we report an important new finding of preserved normal ventricular–ventricular interactions in the setting of acutely increased RV afterload in shunt lambs but not in control or LPA ligation animals. We previously demonstrated the unique ability of the right ventricle in the shunt CHD model to augment contractility in the setting of an acute afterload stimulus due to PA banding (20). In the present study, we have again demonstrated preserved ventricular–vascular coupling and increased RV contractility in only shunt lambs in response to a different acute RV afterload stimulus, U46619, which we hypothesize

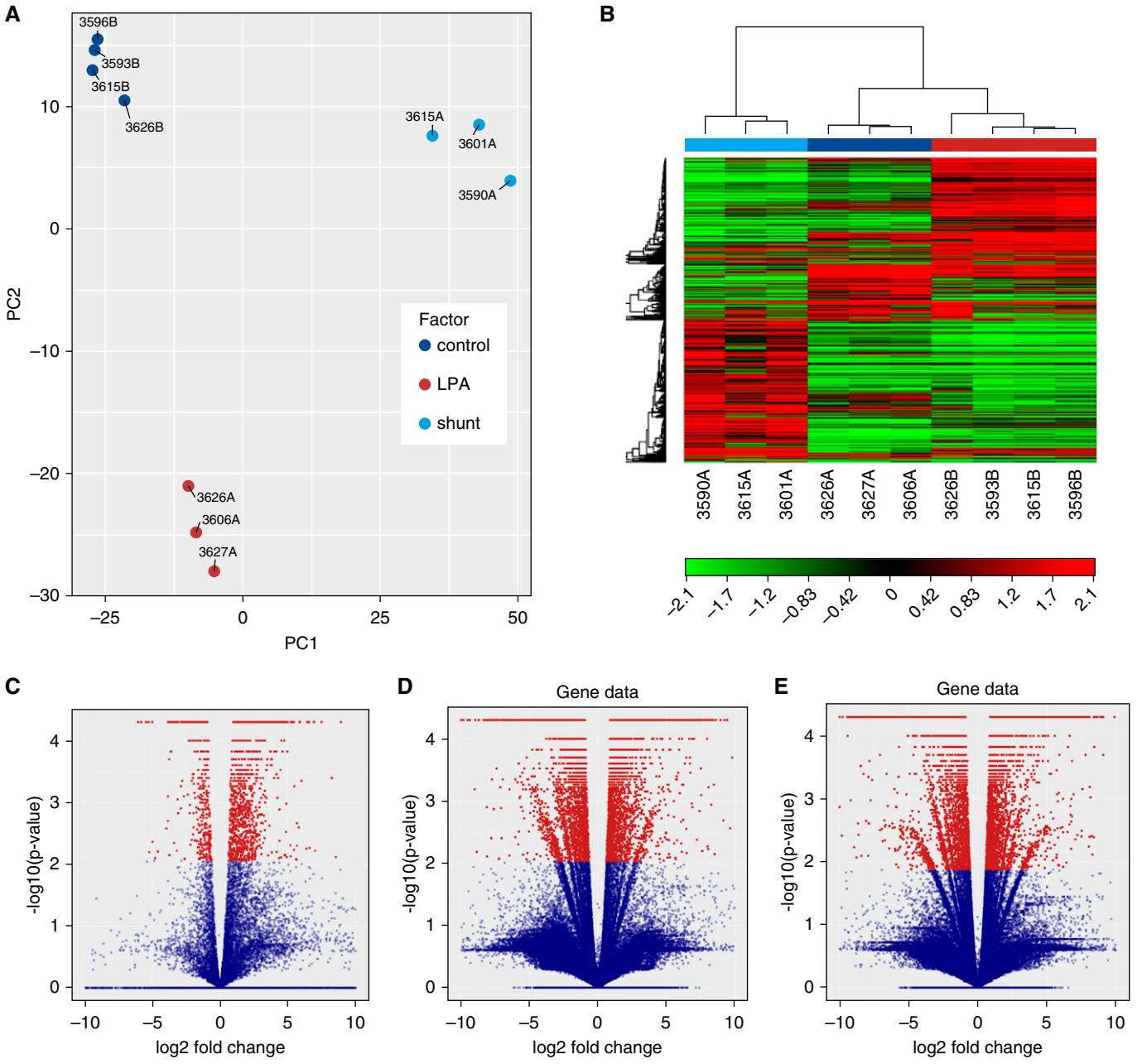

Figure 5. Transcriptional characterization of control, LPA, and shunt pulmonary artery endothelial cells. $N = 4$ control, $n = 3$ LPA, and $n = 3$ shunt. (*A*) Principal clustering (PC) analysis and (*B*) heat map of pulmonary artery endothelial cell RNA-sequencing data confirm clustering of gene expression by model. (*C–E*) Volcano plots of differentially expressed genes are plotted for $\log_2$ fold change versus $-\log_{10} P$ value. Points shown in red have a P value less than 0.05. Volcano plots shown are for (*C*) control versus LPA, (*D*) control versus shunt, and (*E*) LPA versus shunt.

is a consequence of ongoing postnatal exposure of the shunt RV to increased PA pressure. Thus, the similar behavior of the RV in both control and LPA ligation models is expected, given similar postnatal hemodynamic forces on the right ventricle. Importantly, simultaneous biventricular pressure–volume loops have newly demonstrated these advantageous effects on ventricular–ventricular interactions. Impaired early diastolic LV filling is an important and perilous clinical hallmark of RV failure. In the case of both control and LPA animals, the left ventricle demonstrates diastolic dysfunction as visualized by alteration in the LV volume curve and quantified by LV stiffness. Together, these findings demonstrate the increased resilience of the right ventricle–pulmonary vascular unit primed developmentally by chronically increased pressure and flow to acute afterload stimuli, in contrast to the typical vulnerability of the unconditioned right ventricle (35) to overcome sudden increases in afterload seen in both LPA and control lambs.

This study has several important limitations. Perhaps most important, hemodynamic data demonstrate a slight

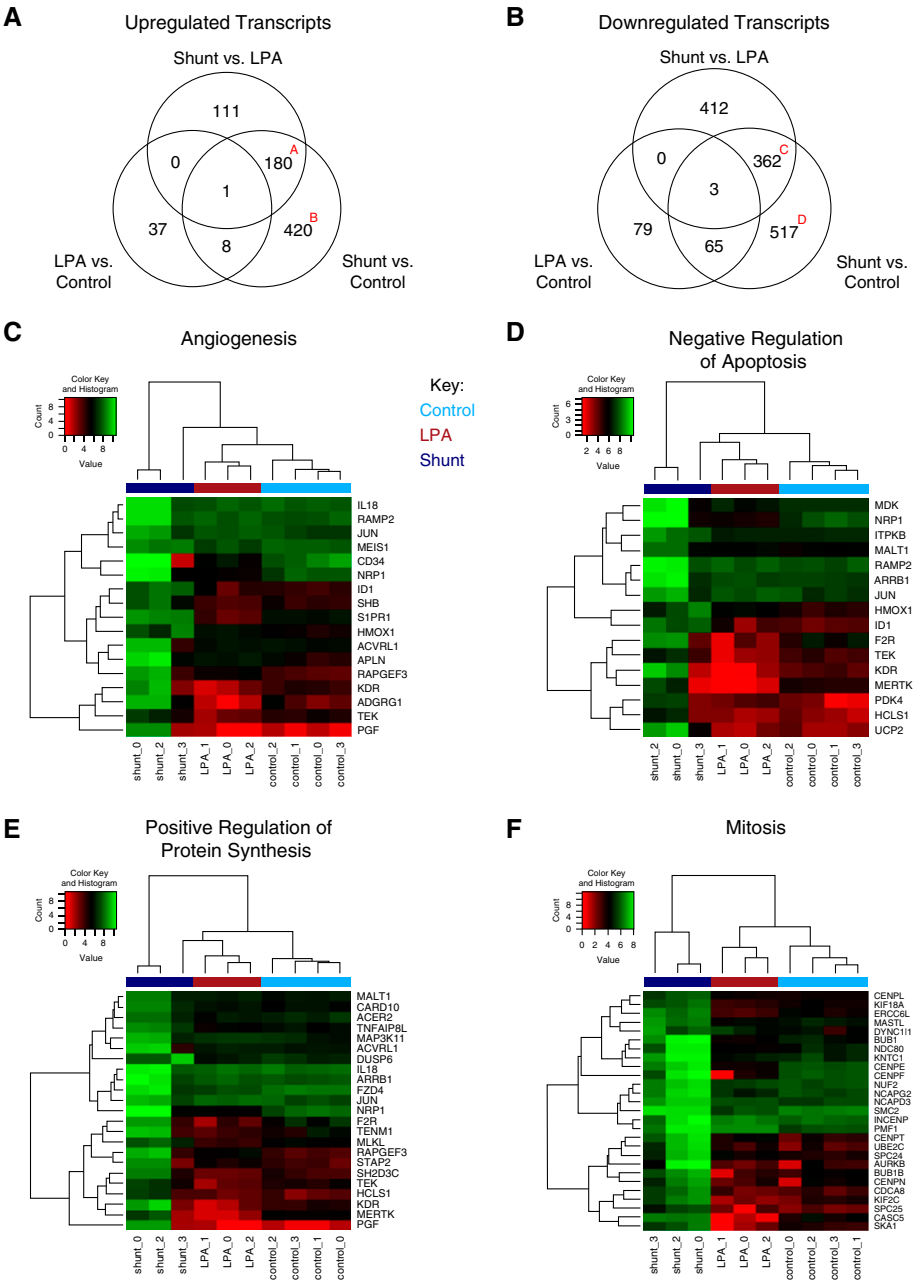

Figure 6. RNA-sequencing analysis. Venn diagrams demonstrate overlapping and distinct changes in (*A*) upregulated and (*B*) downregulated differentially expressed transcripts (DETs) among control, LPA, and shunt models. The 180 genes highlighted by red *A* represent the differentially expressed genes (DEGs) shared in the comparison of shunt versus LPA and shunt versus control pulmonary artery endothelial cells (PAECs). These DEGs are upregulated in shunt PAECs relative to both control and LPA cells and indicate changes to PAEC gene expression that are unique to cells exposed to increased pressure and flow. See pathway analysis of these genes (panels *C–F*). Contrastingly, red *B* represents the 420 DEGs that were significantly upregulated in shunt PAECs relative to control cells. While these genes also indicate transcriptional changes that might be induced by increased pressure and flow, their activated expression is not statistically different from what is observed in LPA cells (or else they would be in the *A* bubble). See pathway analysis of these genes (panels *C–F*). Further details of enriched pathways in these DETs can be found in Tables E5 and E6 in the data supplement. To characterize biological processes represented by these DETs, the Gene Ontology database was used to characterize these changes. Upregulated DETs mapped to processes implicated in pulmonary vascular disease, including (*C*) angiogenesis and vascular development, (*D*) negative regulation of apoptotic processes, (*E*) positive regulation of cellular protein metabolism, and (*F*) mitosis. Red *C* is similar to red *A* in that it represents the downregulated DEGs shared in the comparison of shunt versus LPA and shunt versus control PAECs. These DEGs are downregulated in shunt PAECs relative to both control and LPA cells and indicate changes to PAEC gene expression that are unique to cells exposed to increased pressure and flow. See pathway analysis of these genes (panels *C–F*). Red *D* is similar to red *B* in that it represents the downregulated DEGs downregulated in shunt PAECs relative to control cells. See pathway analysis of these genes (panels *C–F*). These comparative changes among models are shown using supervised clustering heat maps with consistently demonstrated clustering among models. $n = 4$ control, $n = 3$ LPA, and $n = 3$ shunt.

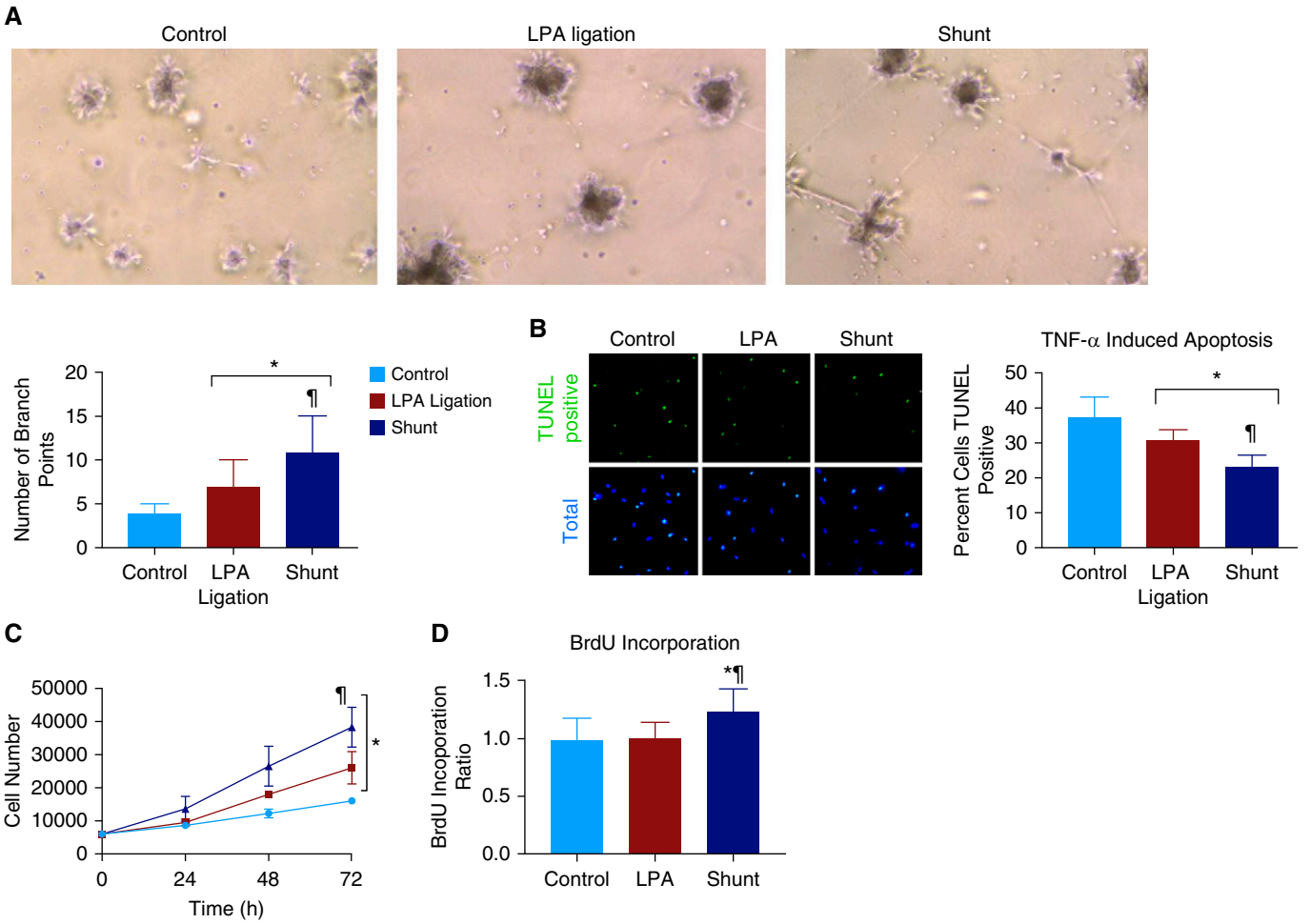

Figure 7. Pulmonary artery endothelial cell (PAEC) functional characteristics: angiogenesis, apoptosis, and proliferation. (*A*) PAECs' angiogenic capacity was assessed using Matrigel assay. Both LPA and shunt PAECs formed a greater number of branch points than did PAECs isolated from control lambs, whereas shunt PAECs had an even greater number of branch points than did PAECs derived from LPA lambs. $n = 5$ per group. (*B*) Apoptosis tendency was quantified using TUNEL assay after TNF-α treatment to induce apoptosis. PAECs from LPA animals had less apoptosis than did PAECs from control lambs (31 ± 2.6% vs. 37.5 ± 5.6% TUNEL positive, respectively), and shunt PAECs had even less apoptosis than PAECs from either LPA or control animals (23.4 ± 3.1% TUNEL positive). Finally, PAEC proliferation was quantified using cell counting and 5′-bromo-2′-deoxyuridine (BrdU) incorporation after 72 hours. (*C*) Proliferation of primary PAECs derived from control, LPA, and shunt animals compared by cell proliferation assay to determine cell counts for primary PAECs. (*D*) BrdU incorporation was greater (1.24 ± 0.2–fold control) at 72 hours among shunt PAECs, compared with both LPA and control PAECs ($n = 3$ per group). Error bars represent ± SD. *$P < 0.05$ compared with control and ¶$P < 0.05$ compared with LPA.

increase in mean PAP in LPA animals compared with control animals, although this model is used primarily to elicit the effects of increased PBF alone. Importantly, the pulmonary vasculature of shunt animals is exposed to a direct systemic pressure stimulus via the aortopulmonary shunt; in contrast, the slight elevation in PAP seen in LPA lambs is due to developed pressure as a consequence of increased PBF in a single-lung vascular bed. In addition, the pulmonary pulse pressure (the difference between diastolic and systolic pressures) is elevated only in shunt animals and not in LPA animals. This alteration in pulse pressure translates into increased cyclic stretch on the pulmonary vasculature. An additional important limitation is that although PVD due to CHD clearly has an ongoing developmental component, these animals were only studied at a single developmental time point, 4–6 weeks of age. Increased developmental elucidation of these models warrants further study, but this 4–6 weeks time point is well characterized in the shunt animal, in terms of both biochemical mechanisms underlying early pulmonary endothelial dysfunction (36–39) and adaptive RV responses (20, 40). Thus, this time point was the most logical for comparison with the new LPA ligation model. Furthermore, the PAECs in this study were cultured from the proximal conducting pulmonary arteries. Additional studies are warranted that focus on the effect of these differing hemodynamic forces on microvascular endothelial cells. Finally, this study is limited by the lack of a unifying biochemical mechanism apart from significant alterations in mechanical forces. As noted, there are potential clues within our RNA-sequencing dataset indicating underlying mechanisms that warrant further confirmatory study.

In conclusion, through the introduction of a new model of CHD with increased PBF alone (fetal LPA ligation),

we were able to investigate the differential and additive effects of common hemodynamic alterations in the pulmonary vasculature as a consequence of CHD: increased PBF and increased PAP. Given the significant burden of PVD among patients with CHD, particularly in the pediatric population, a fundamental understanding of the differing mechanisms leading to vascular pathology associated with different CHD lesions provides an essential tool in tailoring therapy for these patients. As medicine is increasingly focused on personalized and precision medicine approaches, these ovine models of CHD can be leveraged to yield mechanism-specific therapeutic strategies in contrast to current standards of care for pulmonary hypertension therapy that are largely tailored to disease severity. ■

Author disclosures are available with the text of this article at www.atsjournals.org.

Acknowledgment: The authors acknowledge Linda Talken and Rachel Hutchings for their expert husbandry care of our animals.

References

1. Butrous G, Ghofrani HA, Grimminger F. Pulmonary vascular disease in the developing world. *Circulation* 2008;118:1758–1766.
2. Duffels MGJ, Engelfriet PM, Berger RMF, van Loon RLE, Hoendermis E, Vriend JWJ, *et al*. Pulmonary arterial hypertension in congenital heart disease: an epidemiologic perspective from a Dutch registry. *Int J Cardiol* 2007;120:198–204.
3. Adatia I, Kothari SS, Feinstein JA. Pulmonary hypertension associated with congenital heart disease: pulmonary vascular disease: the global perspective. *Chest* 2010;137(Suppl6):52S–61S.
4. Simonneau G, Gatzoulis MA, Adatia I, Celermajer D, Denton C, Ghofrani A, *et al*. Updated clinical classification of pulmonary hypertension. *J Am Coll Cardiol* 2013;62(Suppl25):D34–D41.
5. Kameny RJ, Fineman J, Adatia I. Perioperative management of pediatric pulmonary hypertension. *Adv Pulm Hypertens* 2016;15: 87–91.
6. Steele PM, Fuster V, Cohen M, Ritter DG, McGoon DC. Isolated atrial septal defect with pulmonary vascular obstructive disease – long-term follow-up and prediction of outcome after surgical correction. *Circulation* 1987;76:1037–1042.
7. Webb G, Gatzoulis MA. Atrial septal defects in the adult: recent progress and overview. *Circulation* 2006;114:1645–1653.
8. Haworth SG. Pulmonary vascular disease in different types of congenital heart disease: implications for interpretation of lung biopsy findings in early childhood. *Br Heart J* 1984;52:557–571.
9. Lakier JB, Stanger P, Heymann MA, HoffmaN JI, Rudolph AM. Early onset of pulmonary vascular obstruction in patients with aortopulmonary transposition and intact ventricular septum. *Circulation* 1975;51: 875–880.
10. Abman SH, Hansmann G, Archer SL, Ivy DD, Adatia I, Chung WK, *et al*.; American Heart Association Council on Cardiopulmonary, Critical Care, Perioperative and Resuscitation; Council on Clinical Cardiology; Council on Cardiovascular Disease in the Young; Council on Cardiovascular Radiology and Intervention; Council on Cardiovascular Surgery and Anesthesia; American Thoracic Society. Pediatric pulmonary hypertension: guidelines from the American Heart Association and American Thoracic Society. *Circulation* 2015; 132:2037–2099.
11. Haworth SG, Hislop AA. Treatment and survival in children with pulmonary arterial hypertension: the UK Pulmonary Hypertension Service for Children 2001-2006. *Heart* 2009;95:312–317.
12. Manes A, Palazzini M, Leci E, Bacchi Reggiani ML, Branzi A, Galiè N. Current era survival of patients with pulmonary arterial hypertension associated with congenital heart disease: a comparison between clinical subgroups. *Eur Heart J* 2014;35:716–724.
13. Stevens GR, Garcia-Alvarez A, Sahni S, Garcia MJ, Fuster V, Sanz J. RV dysfunction in pulmonary hypertension is independently related to pulmonary artery stiffness. *JACC Cardiovasc Imaging* 2012;5: 378–387.
14. Gan CTJ, Lankhaar JW, Westerhof N, Marcus JT, Becker A, Twisk JWR, *et al*. Noninvasively assessed pulmonary artery stiffness predicts mortality in pulmonary arterial hypertension. *Chest* 2007; 132:1906–1912.
15. Friesen RM, Schäfer M, Ivy DD, Abman SH, Stenmark K, Browne LP, *et al*. Proximal pulmonary vascular stiffness as a prognostic factor in children with pulmonary arterial hypertension. *Eur Heart J Cardiovasc Imaging* 2018;149:1317.
16. Tan Y, Tseng PO, Wang D, Zhang H, Hunter K, Hertzberg J, *et al*. Stiffening-induced high pulsatility flow activates endothelial inflammation via a TLR2/NF-κB pathway. *PLoS One* 2014;9:e102195.
17. Reddy VM, Meyrick B, Wong J, Khoor A, Liddicoat JR, Hanley FL, *et al*. *In utero* placement of aortopulmonary shunts: a model of postnatal pulmonary hypertension with increased pulmonary blood flow in lambs. *Circulation* 1995;92:606–613.
18. Black SM, Field-Ridley A, Sharma S, Kumar S, Keller RL, Kameny R, *et al*. Altered carnitine homeostasis in children with increased pulmonary blood flow due to ventricular septal defects. *Pediatr Crit Care Med* 2017;18:931–934.
19. Kameny RJ, Zhu T, Morris C, Gong W, Raff GW, Datar SA, *et al*. Pulmonary hypertension associated with congenital heart disease: translating natural history into pathobiology. Presented at the Pediatric Academic Societies Meeting May 6, 2018, Toronto, ON, Canada. Abstract 2635.4.
20. Johnson RC, Datar SA, Oishi PE, Bennett S, Maki J, Sun C, *et al*. Adaptive right ventricular performance in response to acutely increased afterload in a lamb model of congenital heart disease: evidence for enhanced Anrep effect. *Am J Physiol Heart Circ Physiol* 2014;306:H1222–H1230.
21. Kelly LK, Wedgwood S, Steinhorn RH, Black SM. Nitric oxide decreases endothelin-1 secretion through the activation of soluble guanylate cyclase. *Am J Physiol Lung Cell Mol Physiol* 2004;286: L984–L991.
22. van Haaften EE, Wissing TB, Rutten MCM, Bulsink JA, Gashi K, van Kelle MAJ, *et al*. Decoupling the effect of shear stress and stretch on tissue growth and remodeling in a vascular graft. *Tissue Eng Part C Methods* 2018;24:418–429.
23. Thacher TN, Silacci P, Stergiopulos N, da Silva RF. Autonomous effects of shear stress and cyclic circumferential stretch regarding endothelial dysfunction and oxidative stress: an *ex vivo* arterial model. *J Vasc Res* 2010;47:336–345.
24. Paulin R, Michelakis ED. The metabolic theory of pulmonary arterial hypertension. *Circ Res* 2014;115:148–164.
25. Ryan JJ, Archer SL. Emerging concepts in the molecular basis of pulmonary arterial hypertension: part I. Metabolic plasticity and mitochondrial dynamics in the pulmonary circulation and right ventricle in pulmonary arterial hypertension. *Circulation* 2015;131: 1691–1702.
26. Matlung HL, Bakker ENTP, VanBavel E. Shear stress, reactive oxygen species, and arterial structure and function. *Antioxid Redox Signal* 2009;11:1699–1709.
27. Deng Q, Huo Y, Luo J. Endothelial mechanosensors: the gatekeepers of vascular homeostasis and adaptation under mechanical stress. *Sci China Life Sci* 2014;57:755–762.
28. Birukov KG. Cyclic stretch, reactive oxygen species, and vascular remodeling. *Antioxid Redox Signal* 2009;11:1651–1667.
29. Hsieh HJ, Liu CA, Huang B, Tseng AH, Wang DL. Shear-induced endothelial mechanotransduction: the interplay between reactive oxygen species (ROS) and nitric oxide (NO) and the pathophysiological implications. *J Biomed Sci* 2014;21:3.
30. Black SM, Kumar S, Wiseman D, Ravi K, Wedgwood S, Ryzhov V, *et al*. Pediatric pulmonary hypertension: roles of endothelin-1 and nitric oxide. *Clin Hemorheol Microcirc* 2007;37:111–120.
31. Lauth M, Berger MM, Cattaruzza M, Hecker M. Elevated perfusion pressure upregulates endothelin-1 and endothelin B receptor expression in the rabbit carotid artery. *Hypertension* 2000;35:648–654.

32. Duong HT, Comhair SA, Aldred MA, Mavrakis L, Savasky BM, Erzurum SC, *et al*. Pulmonary artery endothelium resident endothelial colony-forming cells in pulmonary arterial hypertension. *Pulm Circ* 2011;1:475–486.
33. Abe K, Toba M, Alzoubi A, Ito M, Fagan KA, Cool CD, *et al*. Formation of plexiform lesions in experimental severe pulmonary arterial hypertension. *Circulation* 2010;121:2747–2754.
34. Voelkel NF, Quaife RA, Leinwand LA, Barst RJ, McGoon MD, Meldrum DR, *et al*.; National Heart, Lung, and Blood Institute Working Group on Cellular and Molecular Mechanisms of Right Heart Failure. Right ventricular function and failure: report of a National Heart, Lung, and Blood Institute working group on cellular and molecular mechanisms of right heart failure. *Circulation* 2006;114:1883–1891.
35. Chin KM, Coghlan G. Characterizing the right ventricle: advancing our knowledge. *Am J Cardiol* 2012;110(Suppl6):3S–8S.
36. Reddy VM, Wong J, Liddicoat JR, Johengen M, Chang R, Fineman JR. Altered endothelium-dependent responses in lambs with pulmonary hypertension and increased pulmonary blood flow. *Am J Physiol* 1996;271:H562–H570.
37. Oishi P, Sharma S, Grobe A, Azakie A, Harmon C, Johengen MJ, *et al*. Alterations in cGMP, soluble guanylate cyclase, phosphodiesterase 5, and B-type natriuretic peptide induced by chronic increased pulmonary blood flow in lambs. *Pediatr Pulmonol* 2007;42: 1057–1071.
38. Oishi P, Azakie A, Harmon C, Fitzgerald RK, Grobe A, Xu J, *et al*. Nitric oxide-endothelin-1 interactions after surgically induced acute increases in pulmonary blood flow in intact lambs. *Am J Physiol Heart Circ Physiol* 2006;290:H1922–H1932.
39. Sharma S, Kumar S, Sud N, Wiseman DA, Tian J, Rehmani I, *et al*. Alterations in lung arginine metabolism in lambs with pulmonary hypertension associated with increased pulmonary blood flow. *Vascul Pharmacol* 2009;51:359–364.
40. Kameny RJ, He Y, Morris C, Sun C, Johengen M, Gong W, *et al*. Right ventricular nitric oxide signaling in an ovine model of congenital heart disease: a preserved fetal phenotype. *Am J Physiol Heart Circ Physiol* 2015;309: H157–H165.